Gallium: A Universal Promoters Switching the CO_2 Methanation Catalysts to Produce Methanol

Wei Zhou[a‡], Colin Hansen[a‡], Weicheng Cao[a], Enzo Brack[a], Scott R. Docherty[a], Christian Ehinger[a], Yuhao Wang[b], Chunliang Wang[b], and Christophe Copéret[a*]

[a]*Department of Chemistry and Applied Biosciences, ETH Zürich, CH-8093 Zurich, Switzerland*

[b]*Engineering Research Center of Metallurgical Energy Conservation and Emission Reduction, Ministry of Education, Kunming University of Science and Technology, Kunming 650093, China*

‡These authors contributed equally to this work

*Corresponding author: ccoperet@inorg.chem.ethz.ch

Abstract

Hydrogenation of CO_2 to methanol is foreseen as a key step to close the carbon cycle and enable sustainable development. In this study, we show that introducing Ga into silica-supported nanoparticles based on group 8-9 transition noble metals (*M* = Ru, Os, Rh, and Ir – *M*Ga@SiO_2) switches their reactivity from producing methane (sel. >97%) to producing methanol (50% CH_3OH/DME sel.) alongside CO as the only byproduct. These silica-supported catalysts, prepared via a surface organometallic chemistry approach, consist of small, alloyed and narrowly distributed *M*Ga nanoparticles, as evidenced by X-Ray absorption spectroscopy (XAS) and CO adsorption studies. Notably, detailed *in-situ* XAS and diffuse reflectance FT-IR spectroscopy (DRIFTS) studies complemented with density functional theory (DFT) calculations indicate that Ga generates stable *M*Ga alloys, which persist during CO_2 hydrogenation and favor the formation of methoxyl species, thus driving the overall reaction to methanol formation while suppressing methanation.

INTRODUCTION

CO_2 hydrogenation based on green H_2 is a key technology, which is envisaged to enable a more sustainable chemical industry. This process can yield various products, ranging from CO, via the so-called Reverse Water Gas Shift (RWGS) reaction,[1, 2] to methane by the Sabatier reaction.[3] It can also yield intermediate compounds like methanol or even higher hydrocarbon or alcohol products via the Fischer-Tropsch process.[4-7] However, the hydrogenation of CO_2 towards value-added chemicals like methanol is notoriously more challenging when compared to the hydrogenation of CO, despite both processes sharing common catalytically active materials, reaction conditions and similar reaction mechanisms.[8, 9] The most prominent example is the hydrogenation of CO or CO_2 using Cu-based catalysts, which favor methanol synthesis via formate and methoxy intermediates, while hardly producing methane under a wide range of conditions.[10] Aiming at improving the catalytic performance, large research efforts have been directed at identifying so-called promoters to improve product selectivity. In Cu-based materials, Zn is well-known to greatly enhance methanol selectivity.[10, 11] Other "reducible" elements, in particular Ga, have also been shown to enhance methanol selectivity of Cu-based catalysts.[12-14] Additionally, Ga is able to switch the general reaction outcome. For instance, Ni-catalysts, which under CO_2 hydrogenation conditions are very well-known for their selectivity towards methane, produce methanol at low pressure in the presence of Ga.[15-17] More recently, Ga was reported to even switch the RWGS activity of noble metals like Pd and Pt to methanol formation with exceptional activity.[18-21] Detailed investigations for the PdGa and PtGa-systems using Surface Organometallic Chemistry (SOMC) have shown that redox dynamics involving *M*Ga-GaO_x (*M* = Pd or Pt) interfaces are responsible for promoting methanol formation with high activity.[20, 21]

Considering the well-known methanation activity of group 8-9 transition metals (Ru, Os, Rh, and Ir), [22-25] we thus reasoned, that it was worth exploring how Ga would affect the reactivity patterns and the structure of these metals. Towards this goal, we prepare a series of well-defined, silica-supported *M*Ga@SiO_2 bimetallic catalysts (*M* = Ru, Os, Rh, and Ir) via Surface Organometallic Chemistry, a synthetic approach that generates catalyst structures amenable to detailed (*in-situ*) spectroscopic characterization. Notably, all of the prepared bimetallic catalysts show good selectivity for methanol/DME in CO_2 hydrogenation (selectivity > 50%), while the mono-metallic cases (*M*@SiO_2 catalysts) favor in all cases methanation (CH_4 > 97%). Detailed *in-situ* studies indicate, that Ga readily

forms alloyed *M*Ga nanoparticles for these metals upon H_2 reduction, and that the *M*Ga alloy persists under CO_2 hydrogenation conditions favoring methanol formation, while suppressing methanation. This study highlights the universal propensity of Ga in promoting methanol formation across a broad range of metals, including classical methanation catalysts.

RESULTS

All materials – *M*Ga@SiO_2, *M* = Ru, Os, Rh, Ir – are prepared *via* SOMC approach, in order to enable a better control of the composition and the interface between the metal and the support.[26, 27] The synthesis involves grafting of a molecular precursor on Ga decorated silica, which contains isolated surface –OH groups and Ga^{III} surface sites (Ga^{III}@SiO_2, 0.8 Ga^{III} nm^{-2}). This support material is prepared by grafting of [Ga(OSi(O^tBu)$_3$)$_3$(THF)] on silica, partially dehydroxylated at 700 °C ($SiO_{2\text{-}700}$, 0.9 –OH nm^{-2}), and a subsequent thermal treatment under high vacuum (10^{-5} mbar) to remove all organic residues (Figure S1-2).[28] Then, a metal precursor (Ru, Os, Rh, Ir) is grafted on Ga^{III}@SiO_2, and H_2 treatment of the resulting bimetallic material provides metallic silica-supported nanoparticles (Figure 1a, see ESI for experimental details). The group 8 (Ru/Os) and group 9 (Rh/Ir) metal precursors used for grafting are based on M(*p*-cymene)(OSi(O^tBu)$_3$)$_2$ (Figure S3-5)[29] and M(COD)(DIA) (COD = 1,5-*cis*,*cis*-cyclooctadiene, DIA = N,N'-diisopropylacetamidinate) (Figure S6-12) respectively;[30] they were chosen because they can readily react with surface –OH groups to generate highly dispersed metal sites. In a subsequent treatment under a flow of H_2 at 400 °C, these materials readily generate supported nanoparticles free of organic ligands as evidenced by infrared (IR) spectroscopy (Figure 1b-c, Figure S13-14). The corresponding monometallic materials *M*@SiO_2 (*M* = Ru, Os, Rh, Ir) are also prepared through the same approach, using $SiO_{2\text{-}700}$ in place of Ga^{III}@SiO_2 (Figure S15-18).

The metal loadings in all materials, as determined by inductively coupled plasma optical emission spectroscopy (ICP-OES), are comparable among each other (i.e. within a metal density range of 0.50-0.85 *M*/nm^2) with *M*/Ga ratios close to 1 for *M*Ga@SiO_2 materials (Table S1). HAADF-STEM micrographs show a narrow particle size distribution centered at 1.6-1.8 nm for all four bimetallic *M*Ga@SiO_2 materials (Figure 1d-g). Note that the nanoparticles are smaller for *M*Ga@SiO_2 than for the corresponding *M*@SiO_2, indicating a strong interaction between the transition metal *M* and the Ga promoter (Figure S21-23, Table S1). EDX maps show that the Ga and *M* profiles overlap in all cases, indicating the formation of MGa alloys upon H_2 reduction (Figure S26-29). In fact, IR spectra of the

samples exposed to CO show a significant red-shift of the adsorbed CO on *M*Ga@SiO_2 vs. *M*@SiO_2 (Figure S30),[31, 32] providing further evidence for alloying between *M* and Ga.

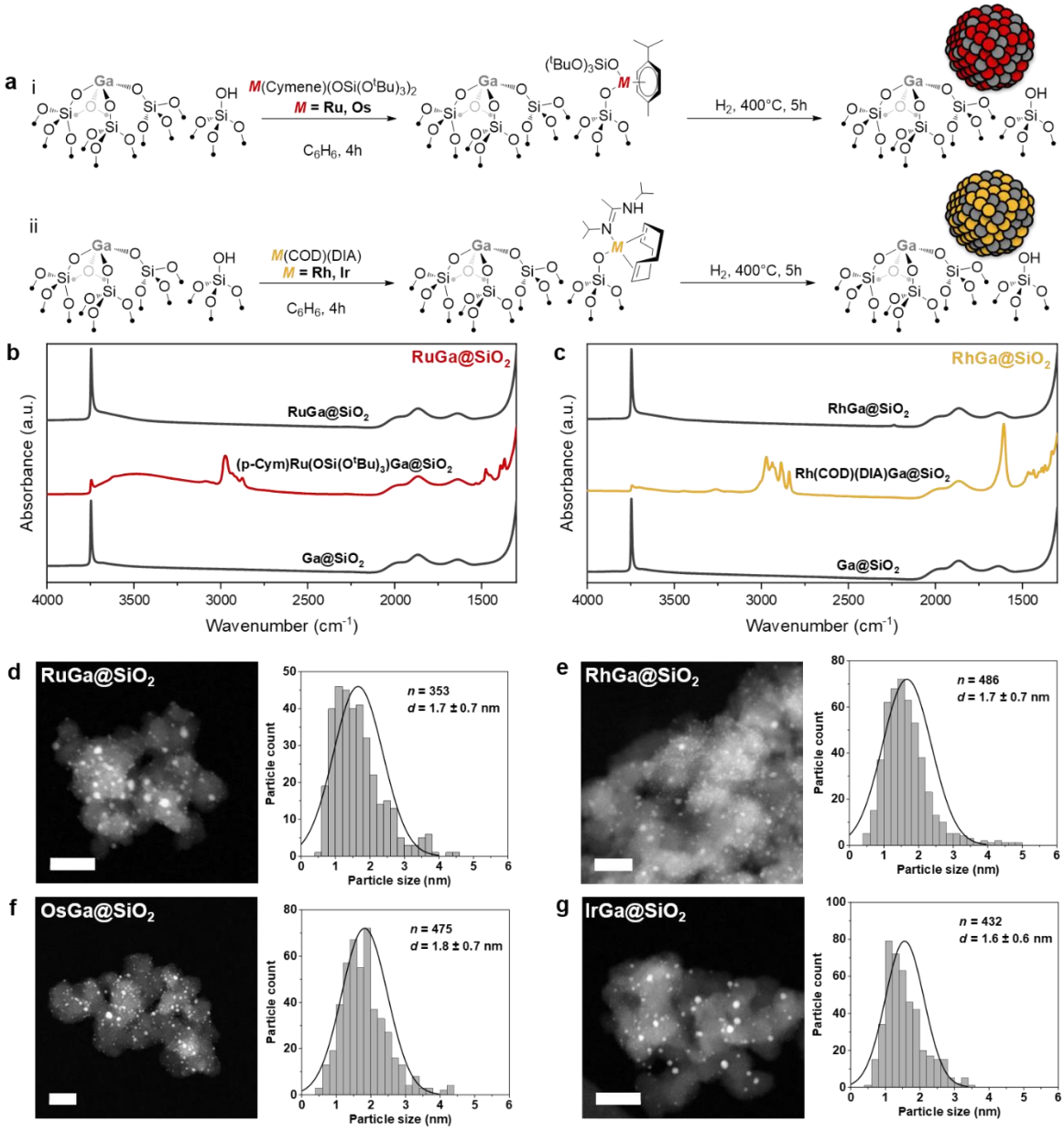

Figure 1. Preparation of *M*Ga@SiO_2 and *M*@SiO_2 materials. a, Schematic procedure for grafting of group 8 (Ru, Os) and group 9 (Rh, Ir) molecular precursors on Ga^{III}@SiO_2 followed by reduction under H_2 at 400 °C. IR spectra throughout the synthesis of RuGa@SiO_2 (b) and RhGa@SiO_2 (c) starting from the second grafting. High-angle annular dark-field STEM (HAADF-STEM) images and particle size distribution of RuGa@SiO_2 (d), RhGa@SiO_2 (e), OsGa@SiO_2 (f) and IrGa@SiO_2 (g). The scale bar measures 20 nm.

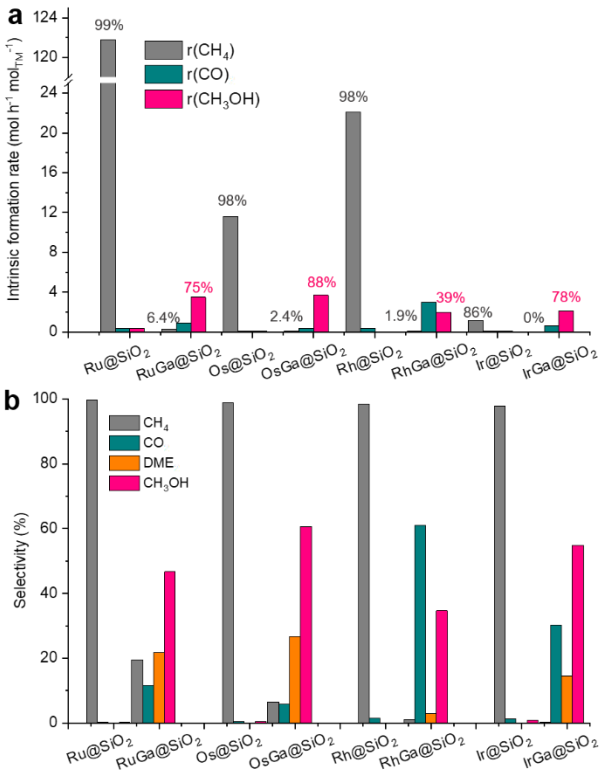

Figure 2. Catalytic performance of CO_2 hydrogenation over investigated catalysts. (a), Intrinsic formation rates over monometallic *M*@SiO_2 and bimetallic *M*Ga@SiO_2 catalysts. (b), Product selectivity over monometallic *M*@SiO_2 and bimetallic *M*Ga@SiO_2 catalysts at CO_2 conversion of 1%. Reaction conditions: F = 6-100 mL/min, T = 230 °C, P = 40 bar.

*M*Ga@SiO_2 and *M*@SiO_2 materials are next evaluated in CO_2 hydrogenation at 230 °C and 40 bar ($H_2/CO_2/Ar$ = 3:1:1). Kinetic information related to product formation is obtained by altering the gas flow rates throughout the experiments. Under the given reaction conditions, methanol is the main product for all the bimetallic catalysts, while monometallic systems produce essentially only methane, with Ga@SiO_2 being inactive (below detection limit) (Figure S31-38). The intrinsic methanol formation rates over RuGa@SiO_2, OsGa@SiO_2, RhGa@SiO_2 and IrGa@SiO_2 are 2.0, 3.7, 2.0 and 2.1 mol h^{-1} mol_{TM}^{-1}, which compare well with other reported CO_2 hydrogenation catalysts prepared by SOMC (Table S3). These rates correspond to intrinsic methanol selectivities of 65%, 88%, 39% and 78% respectively (Figure 2a, Table S2-S3). RhGa@SiO_2 displays the lowest methanol selectivity of 39%, which can be enhanced to approx. 50% upon tuning the Rh/Ga ratio (Figure S19-20, S24-25, S39-42, Table S2). In sharp contrast to bimetallic systems, the corresponding monometallic catalysts – Ru@SiO_2, Os@SiO_2 Rh@SiO_2, and Ir@SiO_2 – produce mainly methane with a relatively high activity and

selectivity, as expected for these metals (Figure 2a, Table S2). It thus becomes evident that Ga significantly suppresses methanation activity, while promoting methanol formation.

Comparing the catalysts at 1% CO_2 conversion shows that the methane selectivity sharply decreases from >97% for monometallic *M*@SiO_2 catalysts to below 20% for Ga-promoted *M*Ga@SiO_2 systems (Figure 2b, Table S4). All four *M*Ga@SiO_2 catalysts also produce CO and a small amount of dimethyl ether (DME). The latter is likely formed due to the dehydration of CH_3OH over Lewis acidic Ga-sites.[12, 20] Overall the selectivity towards CH_3OH/DME lies at 60%, 87%, 38% and 70% for RuGa@SiO_2, OsGa@SiO_2, RhGa@SiO_2 and IrGa@SiO_2, respectively.

To understand the apparent universal promotional effect of Ga, the evolution of structure and chemical properties of all catalysts, except for the Os-based systems, is investigated by *in-situ* X-ray Absorption Spectroscopy (XAS) experiments. In order to do so, XAS spectra are recorded under different conditions (exposed to air, reduced in H_2, post-CO_2 hydrogenation) (Figure S43). The Ga-promoted bimetallic (*M*Ga@SiO_2, *M* = Ru, Rh and Ir) catalysts are investigated at the metal K- or L_3-edge and compared with the monometallic *M*@SiO_2. The corresponding best fits are shown in Figure S44-58 and summarized in Table S5-7. The X-ray absorption near-energy structure (XANES) spectra of the Ru and Rh K-edge for the air-exposed RuGa@SiO_2 and RhGa@SiO_2 catalysts display resemblances to the metal oxide references, while the XANES spectrum at the Ir L_3-edge and the corresponding white line intensity for the air-exposed IrGa@SiO_2 is comparable to metallic Ir foil. A similar difference is observed for the corresponding air-exposed monometallic *M*@SiO_2 catalysts: the XANES spectrum of Ru@SiO_2 is consistent with slightly oxidized metal (Figure S59-60), while Rh@SiO_2 and Ir@SiO_2 remain metallic (Figure S61-64). The extended X-ray absorption fine structure (EXAFS) spectra of both air-exposed RuGa@SiO_2 and RhGa@SiO_2 catalysts reveal a coordination number (CN) of 3.7 and 5.0 for Ru-O and Ru-Ru, and a CN of 2.2 and 4.0 for Rh-O and Rh-Rh, respectively (Figure 3a-d, Figure S47, S50, Table S5-6), indicating a mixture of metallic and oxidized species, consistent with what is observed in XANES. For IrGa@SiO_2 the EXAFS fitting shows a CN of 10.4 for the Ir-Ir scattering path, while no Ir-O path is observed. This further supports the exclusive presence of metallic Ir in the air-exposed IrGa@SiO_2 as found in XANES (Figure 3e-f, Figure S56, Table S7).

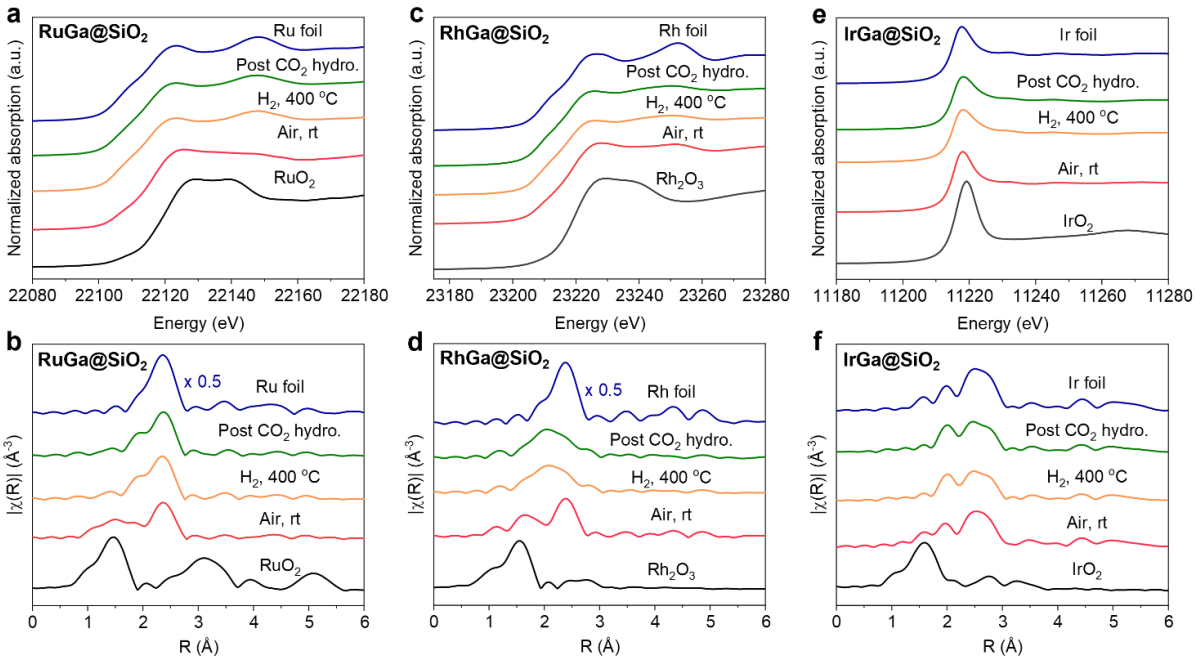

Figure 3. *In situ* XAS studies. XANES spectra and the k^2-weighted Fourier transforms of EXAFS spectra under different conditions for RhGa@SiO_2 at Rh K-edge (a) and (b); RuGa@SiO_2 at Ru K-edge (c) and (d); IrGa@SiO_2, and Ir L_3-edge (e) and (f) respectively.

Next, XANES was used to monitor the evolution of the air-exposed materials throughout H_2 temperature programmed reduction (TPR). With increasing temperatures, the white line intensities at the K-edges of both Ru and Rh gradually decrease and the edge position gradually shifts to lower energy, indicating the reduction of Ru and Rh in both RuGa@SiO_2 and RhGa@SiO_2 (Figure S65a-b). In fact, after H_2 reduction at 400 °C the peaks associated with metal oxides observed in the Fourier transform of the EXAFS spectra disappear, which is again consistent with reduction. Additionally, new peaks appear in the R-space between the ones expected for *M*-O and *M*-*M* (*M* = Ru or Rh) (Figure 3b and 3d), and the EXAFS fitting results for both systems show an average CN of 1.6 and 6.2 for Ru-Ga and Ru-Ru and an average CN of 3.6 and 2.3 for Rh-Ga and Rh-Rh, indicating alloying in both cases (Figure S48, S51, Table S5-6). For IrGa@SiO_2, the Ir L_3-edge XANES spectrum indicates a stepwise shift to higher energy along with a decrease in the white line intensity during H_2 TPR (Figure S65c), which is indicative of a change of structure for Ir due to the presence of Ga. After H_2 reduction, examination of the EXAFS spectrum shows, that the peak at ca. 2.0 Å in R space becomes more intense compared to the second peak at ca. 2.5 Å, while this change is not observed in monometallic Ir@SiO_2 (Figure 3f,

Figure S64). These observations are consistent with the interaction between Ga and Ir, and EXAFS fitting reveals the presence of Ir-Ir scattering path (CN_{Ir-Ir} = 9.2) as well as a Ir-Ga path (CN_{Ir-Ga} = 0.9) (Figure S57, Table S7), thereby confirming IrGa alloy formation upon reduction. Note, that after H_2 reduction of the monometallic *M*@SiO_2 materials at 400°C, the XAS spectra are consistent with the exclusive presence of metallic nanoparticles (Figure S59-64 and S66). EXAFS fitting results after CO_2 hydrogenation indicate similar CN for *M*-Ga in all three *M*Ga@SiO_2 systems, revealing that the *M*Ga alloy persists throughout the CO_2 hydrogenation reaction (Figure 3, Table S5-7). Note that for the monometallic systems, *M* in *M*@SiO_2 remaining fully metallic is well-known for methanation catalysts (Figure S59-64, Table S5-7).

In addition, *in-situ* Ga K-edge XAS spectra were also acquired under the same conditions in order to gain more insights into the interplay between *M* (*M* = Ru, Rh and Ir) and Ga in the *M*Ga@SiO_2 systems. In all cases, the XANES spectra at the Ga K-edge for the air-exposed *M*Ga@SiO_2 systems are similar to Ga^{III}@SiO_2 (Figure S67-69), while the edge position shifts to lower energy and the white line intensity decreases during H_2-TPR (Figure S70). These data suggest, that Ga^{III} is gradually reduced to Ga^0 and incorporated into the nanoparticles to form alloyed *M*Ga nanoparticles after H_2 treatment (vide supra). A linear combination fitting (LCF) analysis of the spectra after H_2 reduction enables us to evaluate the composition of the *M*Ga nanoparticles (Figure S71, Table S8): the average ratios of *M*/Ga^0 are 3.0:1, 1.6:1 and 2.4:1 in RuGa, RhGa and IrGa alloyed nanoparticles respectively, indicating, that the *M*Ga alloys contain ca. 25%-40% of Ga^0. Furthermore, all the Ga K-edge EXAFS spectra can be fitted using a model that includes Ga-O and Ga-*M* paths after H_2 reduction (Figure S72-80, Table S9). Both the *M* K- or L_3-edge and Ga K-edge spectra demonstrate the formation of a *M*-Ga alloy after H_2 reduction. Similar to what is found at corresponding metal *M* edges, no change is observed at the Ga K-edge under CO_2 hydrogenation (Table S9), consistent with the stability of the alloy under these conditions. Overall, the XAS study at both *M* and Ga edges shows that alloying between the metal and Ga is favored under H_2 and that the alloys are stable under CO_2 hydrogenation conditions. This observation parallels the reactivity switch from methanation over pure metal *M* catalysts to methanol formation over *M*Ga alloys.

In-situ Diffuse Reflectance IR Fourier Transform Spectroscopy (DRIFTS) experiments were performed to monitor intermediate species over the Ga-promoted *M*Ga@SiO_2 catalysts (*M* = Ru, Os, Rh, and Ir) and monometallic *M*@SiO_2 during CO_2 hydrogenation at 20 bars. Notably, when the

bimetallic catalysts are exposed to a gas mixture of H_2/CO_2/Ar (3:1:1 – 20 bar), two CO IR bands at 2040-2070 cm^{-1} and 1930-2000 cm^{-1} appear, indicating the presence of two families of CO surface sites. A recent report on related silica-supported PtGa catalysts has indicated, that these two species are likely associated with CO* absorbed on *M*Ga and *M*Ga-GaO_x interfaces. However, direct evidence for the formation of MGa-GaO_x interfaces is not observed by XAS, indicating that the amount of formed MGa-GaO_x interfaces is likely very low (surface domains).[21] In addition, a band at 2170 cm^{-1} (gaseous CO) and a band at 3015 cm^{-1} (gaseous CH_4) can be observed for the *M*Ga@SiO_2 catalysts (Figure S81).[33] Besides the observed bands for gaseous CO and CH_4 and the adsorbed CO*, two bands at around 2960 cm^{-1} and 2858 cm^{-1} are also detected. These two bands can be assigned to methoxy (CH_3O*) species at the surface of the catalysts, which are key intermediates for methanol formation.[20, 34] These methoxy species are not observed over monometallic Ru@SiO_2 and Rh@SiO_2 catalysts. However, a rather high intensity band at 3015 cm^{-1} along with weak rotational bands between 2600-3200 cm^{-1} are observed due to a high concentration of gaseous CH_4 (Figure S82).[35] This is consistent with the observed high methanation activity in CO_2 hydrogenation over Ru@SiO_2 and Rh@SiO_2. The same trend is also observed over Os-based and Ir-based catalysts. Note that slight methoxy bands can be detected after 30 min over Ir@SiO_2, which agrees with the observation that Ir@SiO_2 shows a non-negligible 7% intrinsic methanol selectivity (Figure 2a, Table S2).

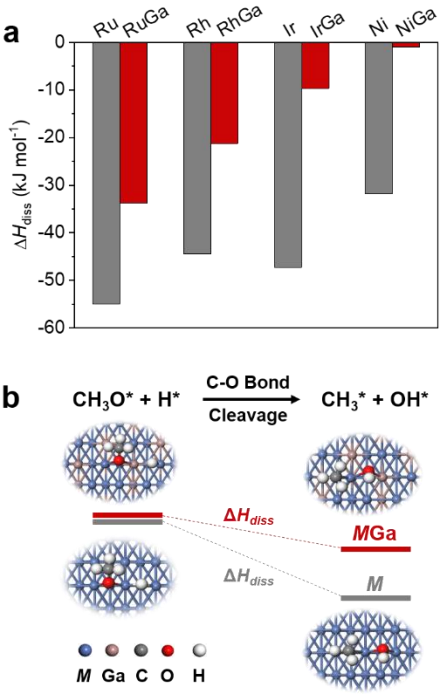

Figure 4. DFT calculation studies. (a) The dissociation enthalpies of C-O in methoxy on the representative facet

of different monometallic *M* and bimetallic *M*Ga (*M* = Ru, Rh, Ir and Ni) systems based on face-centered cubic (FCC) structure. (b) The scheme for cleaving the C-O bond of CH_3O* in the presence of H* on monometallic *M* and bimetallic *M*Ga.

To better understand the affinity of these metals towards alloying with Ga and how alloying prevents methanation, we further explore simple descriptors for alloying and for the capacity towards C-O bond cleavage on pure metals vs. alloyed surfaces using density functional theory (DFT) modelling. The affinity of the various metals towards Ga is evaluated by calculating the alloy formation enthalpy ($\Delta H_{alloying}$). In addition to the metals investigated in this study, we include Ni as a benchmark because it is a well-known methanation catalyst, for which the presence of Ga has been shown to have similar promotional effects, yielding methanol under CO_2 hydrogenation conditions.[17] Osmium however, has been excluded due to the lack of experimental data (no XAS data, *vide supra*) and established work function datasets.

For all the systems, a *M*/Ga (*M* = Ru, Rh, Ir and Ni) ratio of 3:1, close to the experimental ratio quantified by LCF analysis, is used for modelling the alloys. The most stable FCC phase is used as a reference, because it is the most stable metallic state across the selected metals. This phase is chosen to evaluate the alloy formation enthalpy ($\Delta H_{alloying}$) by the energy difference between the metal and corresponding alloy with a similar structure. In all four *M*Ga bimetallic systems, the values of $\Delta H_{alloying}$ are negative (Figure S83-87, Table S10), indicating that Ga is readily incorporated into the *M* phase to form stable *M*Ga alloys for these metals, aligning with the *in-situ* XAS results.

In-situ DRIFTS indicates the presence of methoxy-species during the reaction over bimetallic MGa@SiO_2 catalysts while mostly methane is detected for M@SiO_2. We evaluate the propensity of C-O bond cleavage in an adsorbed methoxy species in the presence of H adatoms on various metal surfaces using a representative {211} facet based on an FCC structure as a simple descriptor (Figure S88). Strongly negative dissociation enthalpies (ΔH_{diss}) hint towards facilitated C-O bond cleavage, while less negative values indicate a higher activation barrier for C-O cleavage and therefore higher probability for methanol formation. As shown in Figure 4, Figure S89-96 and Table S11 the dissociation energy of C-O on monometallic systems is substantially more negative than in *M*Ga systems, suggesting that the cleavage of C-O yielding CH_3* species (which can be readily converted to CH_4) is more favorable on monometallic systems. In contrast, the presence of Ga in bimetallic *M*Ga alloys significantly weakens

the capacity of C-O cleavage, thus stabilizing the methoxy species and promoting methanol formation. Combined with the *in-situ* studies, we propose that the retention of the *M*Ga alloy during the CO_2 hydrogenation is key to suppressing the methanation reaction, while stabilizing the methoxy species and consequently promoting the formation of methanol.

Conclusion

This work shows that Ga displays a unique promotional effect, in that it can switch the catalytic reactivity of classical methanation catalysts, here group 8 and 9 noble metal – Ru/Os and Rh/Ir – silica-supported nanoparticles, to favoring methanol synthesis under classical CO_2 hydrogenation conditions. The addition of Ga significantly decreases the rate of methanation in favor of the formation of oxygenates, in particular methanol and DME. *In-situ* XAS studies indicate, that the non-promoted monometallic *M* systems remain fully metallic under CO_2 hydrogenation conditions and therefore present high activity for the methanation reaction. In contrast, the introduction of Ga generates *M*Ga alloys, which are stable under CO_2 hydrogenation conditions. *In-situ* DRIFTS experiments and DFT calculations evidence that the presence of a stable *M*Ga alloy is critical for stabilizing methoxy species and to promote methanol formation. These observations highlight how promoters can change the state and reactivity of transition-metal elements and provide possible guideline principle to developed methanol synthesis catalysts.

Supporting Information Additional Details for catalysts synthesis, crystal structures, routine characterization, DFT calculations and catalytic tests have been included in the Supporting Information.

Acknowledgements This publication was created as part of NCCR Catalysis (grant number 180544), a National Centre of Competence in Research funded by the Swiss National Science Foundation. C. C. and S. R. D. acknowledge the Swiss National Science Foundation (grants 200021_169134, and 200020B_192050), while C. E. acknowledges the Swiss National Science Foundation (grant 200020B_192050) and the Scholarship Fund of the Swiss Chemical Industry (SSCI). Prof. Dr. A. Comas-Vives is thanked for the scientific discussion on DFT studies, and Prof. Dr. M. P. Conley is thanked for developing the Ru precursor. The authors acknowledge Dr W. V. Beek and Dr D. Stoian at the Swiss Norwegian Beamlines (SNBL, ESRF) for the provision of beamtime and support with *in situ* XAS experiments *via* proposal A31-1-168 and A31-1-197. X. Zhou and K. Sakamoto are thanked for

supporting experiment at the synchrotron. Furthermore, ScopeM is gratefully acknowledged for their support and assistance in this work through project No. 2658. Crystal Data for Ru(*p*-Cymene)(OSi(O^{t}Bu)$_3$)$_2$, Os(*p*-Cymene)(OSi(O^{t}Bu)$_3$)$_2$ and Ir(COD)(DIA) can be obtained free of charge from Cambridge Crystallographic Data Centre (CCDC number: 2330054, 2329726 and 2329723)

Author Contributions W.Z., and C.C. conceived and designed the study. C.C. supervised the project. W.Z. and C.H. performed the catalyst preparation, catalytic reactions and most of characterizations. W.C. performed the theoretical calculation. E.B. performed the TEM experiments. Y.W. and C.W. performed the DRIFTS experiments. S.D. and C.E. assisted in in situ XAS and metal precursors synthesis. W.Z., C.H. and C.C. co-wrote the manuscript.

Author Information The authors declare no competing interest. Correspondence and requests for materials should be addressed to ccoperet@inorg.chem.ethz.ch.

References

1. Khoshooei M. A.; Wang X.; Vitale G.; Formalik F.; Kirlikovali K. O.; Snurr R. Q.; Pereira-Almao P.; K., F. O., An active, stable cubic molybdenum carbide catalyst for the high-temperature reverse water-gas shift reaction. *Science* **2024,** *384*, 540–546

2. Szenti I.; Efremova A.; Kiss J.; Sapi A.; Ovari L.; Halasi G.; Haselmann U.; Zhang Z.; Morales-Vidal J.; Baan K.; Kukovecz A.; Lopez N.; Konya Z., Pt/MnO Interface Induced Defects for High Reverse Water Gas Shift Activity. *Angew. Chem. Int. Ed.* **2023**, e202317343.

3. Vogt C.; Monai M.; Kramer G. J.; Weckhuysen B. M., The renaissance of the Sabatier reaction and its applications on Earth and in space. *Nat. Catal.* **2019,** *2*, 188-197.

4. Kattel, S.; Ramírez, P. J.; Chen, J. G.; Rodriguez, J. A.; Liu, P., Active sites for CO2 hydrogenation to methanol on Cu/ZnO catalysts. *Science* **2017,** *355* (6331), 1296-1299.

5. Behrens, M.; Studt, F.; Kasatkin, I.; Kühl, S.; Hävecker, M.; Abild-Pedersen, F.; Zander, S.; Girgsdies, F.; Kurr, P.; Kniep, B.-L.; Tovar, M.; Fischer, R. W.; Nørskov, J. K.; Schlögl, R., The Active Site of Methanol Synthesis over Cu/ZnO/Al2O3 Industrial Catalysts. *Science* **2012,** *336* (6083), 893-897.

6. Zhou W.; Cheng K.; Kang J.; Zhou C.; Subramanian V.; Zhang Q.; Wang Y., New horizon in

C1 chemistry: breaking the selectivity limitation in transformation of syngas and hydrogenation of CO2 into hydrocarbon chemicals and fuels. *Chem. Soc. Rev.* **2019,** *48*, 3193-3228.

7. Xu, D.; Wang, Y.; Ding, M.; Hong, X.; Liu, G.; Tsang, S. C. E., Advances in higher alcohol synthesis from CO2 hydrogenation. *Chem* **2021,** *7* (4), 849-881.

8. Zhong, J.; Yang, X.; Wu, Z.; Liang, B.; Huang, Y.; Zhang, T., State of the art and perspectives in heterogeneous catalysis of CO_2 hydrogenation to methanol. *Chem. Soc. Rev.* **2020,** *49* (5), 1385-1413.

9. Jiang, X.; Nie, X.; Guo, X.; Song, C.; Chen, J. G., Recent advances in carbon dioxide hydrogenation to methanol via heterogeneous catalysis. *Chem. Rev.* **2020,** *120* (15), 7984-8034.

10. Beck A.; Newton M. A.; van de Water L. G. A.; van Bokhoven J. A., The Enigma of Methanol Synthesis by Cu/ZnO/Al(2)O(3)-Based Catalysts. *Chem. Rev.* **2024,** *124* (8), 4543-4678.

11. Lam, E.; Noh, G.; Larmier, K.; Safonova, O. V.; Copéret, C., CO_2 hydrogenation on Cu-catalysts generated from ZnII single-sites: Enhanced CH_3OH selectivity compared to $Cu/ZnO/Al_2O_3$. *J. Catal.* **2021,** *394*, 266-272.

12. Lam, E.; Noh, G.; Chan, K. W.; Larmier, K.; Lebedev, D.; Searles, K.; Wolf, P.; Safonova, O. V.; Coperet, C., Enhanced CH_3OH selectivity in CO_2 hydrogenation using Cu-based catalysts generated via SOMC from Ga(III) single-sites. *Chem. Sci.* **2020,** *11* (29), 7593-7598.

13. Hong S.; Reddy K. P.; Song Y.; Park D.; Park J. Y., Enhanced methanol formation in CO_2 hydrogenation through synergistic copper and gallium interaction. *J. Catal.* **2024,** *437*, 115643.

14. Schumann, J.; Eichelbaum, M.; Lunkenbein, T.; Thomas, N.; Álvarez Galván, M. C.; Schlögl, R.; Behrens, M., Promoting strong metal support interaction: Doping ZnO for enhanced activity of Cu/ZnO:M (M = Al, Ga, Mg) catalysts. *ACS Catal.* **2015,** *5* (6), 3260-3270.

15. Studt, F.; Sharafutdinov, I.; Abild-Pedersen, F.; Elkjær, C. F.; Hummelshøj, J. S.; Dahl, S.; Chorkendorff, I.; Nørskov, J. K., Discovery of a Ni-Ga catalyst for carbon dioxide reduction to methanol. *Nat. Chem.* **2014,** *6* (4), 320-324.

16. Sharafutdinov, I.; Elkjær, C. F.; Pereira de Carvalho, H. W.; Gardini, D.; Chiarello, G. L.; Damsgaard, C. D.; Wagner, J. B.; Grunwaldt, J.-D.; Dahl, S.; Chorkendorff, I., Intermetallic compounds of Ni and Ga as catalysts for the synthesis of methanol. *J. Catal.* **2014,** *320*, 77-88.

17. Zimmerli N. K.; Rochlitz L.; Checchiac S.; Müller C. R.; Copéret C.; M., A. P., Structure and role of a Ga-promoter in Ni-based catalysts for the selective hydrogenation of CO_2 to Methanol. *JACS Au* **2024,** *4*, 237-252.

18. García-Trenco, A.; White, E. R.; Regoutz, A.; Payne, D. J.; Shaffer, M. S. P.; Williams, C. K., Pd_2Ga-based colloids as highly active catalysts for the hydrogenation of CO_2 to methanol. *ACS Catal.* **2017,** *7* (2), 1186-1196.

19. Liu, X.; Gu, Q.; Zhang, Y.; Xu, X.; Wang, H.; Sun, Z.; Cao, L.; Sun, Q.; Xu, L.; Wang, L.; Li, S.; Wei, S.; Yang, B.; Lu, J., Atomically thick oxide overcoating stimulates low-temperature reactive metal-support interactions for enhanced catalysis. *J. Am. Chem. Soc.* **2023,** *145* (12), 6702-6709.

20. Docherty, S. R.; Phongprueksathat, N.; Lam, E.; Noh, G.; Safonova, O. V.; Urakawa, A.; Coperet, C., Silica-supported PdGa nanoparticles: metal synergy for highly active and selective CO_2 to CH_3OH hydrogenation. *JACS Au* **2021,** *1* (4), 450-458.

21. Zhou, W.; Brack, E.; Ehinger, C.; Paterson, J.; Southouse, J.; Coperet, C., Reactivity Switch of Platinum with Gallium: From Reverse Water Gas Shift to Methanol Synthesis. *J. Am. Chem. Soc.* **2024,** *146* (15), 10806-10811.

22. Wang, F.; He, S.; Chen, H.; Wang, B.; Zheng, L.; Wei, M.; Evans, D. G.; Duan, X., Active Site Dependent Reaction Mechanism over Ru/CeO_2 Catalyst toward CO_2 Methanation. *J. Am. Chem. Soc.* **2016,** *138* (19), 6298-305.

23. Jackson S. D. ; Moyes R. B.; Wells P. B.; Whyman R., Chemisorption and catalysis by metal clusters: III. Hydrogenation of ethene, carbon monoxide, and carbon dioxide, and hydrogenolysis of ethane catalyzed by supported osmium clusters derived from $Os_3(CO)_{12}$ and from $Os_6(CO)_{18}$. *J. Catal.* **1984,** *86* (2), 342-358.

24. Wang C.; Guan E.; Wang L.; Chu X. ; Wu Z.; Zhang J.; Yang Z; Jiang Y.; Zhang L. ; Meng X.; Gates B. C.; Xiao F. S., Product Selectivity Controlled by Nanoporous Environments in Zeolite Crystals Enveloping Rhodium Nanoparticle Catalysts for CO_2 Hydrogenation. *J. Am. Chem. Soc.* **2019,** *141* (21), 8482-8488.

25. Li, S.; Xu, Y.; Chen, Y.; Li, W.; Lin, L.; Li, M.; Deng, Y.; Wang, X.; Ge, B.; Yang, C.; Yao, S.; Xie, J.; Li, Y.; Liu, X.; Ma, D., Tuning the selectivity of catalytic carbon dioxide hydrogenation over iridium/cerium oxide catalysts with a strong metal–support interaction. *Angew. Chem. Int. Ed.* **2017,** *56* (36), 10761-10765.

26. Coperet, C.; Comas-Vives, A.; Conley, M. P.; Estes, D. P.; Fedorov, A.; Mougel, V.; Nagae, H.; Nunez-Zarur, F.; Zhizhko, P. A., Surface organometallic and coordination chemistry toward single-site heterogeneous catalysts: Strategies, methods, structures, and activities. *Chem. Rev.* **2016,** *116* (2), 323-421.

27. Docherty, S. R.; Coperet, C., Deciphering metal-oxide and metal-metal interplay via surface organometallic chemistry: A case study with CO_2 hydrogenation to methanol. *J. Am. Chem. Soc.* **2021,** *143* (18), 6767-6780.

28. Searles, K.; Siddiqi, G.; Safonova, O. V.; Copéret, C., Silica-supported isolated gallium sites as highly active, selective and stable propane dehydrogenation catalysts. *Chem. Sci.* **2017,** *8* (4), 2661-2666.

29. Heroguel, F. E., Controlled growth and inerfaces of supported metal nanoparticles from late transition metal siloxides. *ETH DISS. NO 21918* **2014**.

30. Zhou, W.; Docherty, S. R.; Ehinger, C.; Zhou, X.; Coperet, C., The promotional role of Mn in CO_2 hydrogenation over Rh-based catalysts from a surface organometallic chemistry approach. *Chem. Sci.* **2023,** *14* (20), 5379-5385.

31. Elgayyar, T.; Atwi, R.; Tuel, A.; Meunier, F. C., Contributions and limitations of IR spectroscopy of CO adsorption to the characterization of bimetallic and nanoalloy catalysts. *Catal. Today* **2021,** *373*, 59-68.

32. Nakaya, Y.; Furukawa, S., Catalysis of alloys: Classification, principles, and design for a variety of materials and reactions. *Chem. Rev.* **2023,** *123* (9), 5859-5947.

33. Mojet, B. L.; Ebbesen, S. D.; Lefferts, L., Light at the interface: the potential of attenuated total reflection infrared spectroscopy for understanding heterogeneous catalysis in water. *Chem. Soc. Rev.* **2010,** *39* (12), 4643-4655.

34. Collins, S. E.; Briand, L. E.; Gambaro, L. A.; Baltanás, M. A.; Bonivardi, A. L., Adsorption and decomposition of methanol on gallium oxide polymorphs. *J. Phys. Chem. C* **2008,** *112* (38), 14988-15000.

35. Esler, M. B.; Griffith, D. W. T.; Wilson, S. R.; Steele, L. P., Precision trace gas analysis by FT-IR spectroscopy. 1. simultaneous analysis of CO_2, CH_4, N_2O, and CO in Air. *Anal. Chem.* **2000,** *72* (1), 206-215.

Entry for the Table of Contents